Chinese Journal of Chemical Engineering 56 (2023) 25–32

Contents lists available at ScienceDirect

Chinese Journal of Chemical Engineering

journal homepage: www.elsevier.com/locate/CJChE

Full Length Article

A Ruddlesden–Popper oxide as a carbon dioxide tolerant cathode for solid oxide fuel cells that operate at intermediate temperatures

Shujun Peng [1], Song Lei [2], Sisi Wen [2], Jian Xue [2,*], Haihui Wang [3]

[1] School of Chemistry & Chemical Engineering, Jinggangshan University, Ji'an 343009, China
[2] School of Chemistry & Chemical Engineering, Guangdong Provincial Key Lab of Green Chemical Product Technology, South China University of Technology, Guangzhou 510640, China
[3] Beijing Key Laboratory of Membrane Materials and Engineering, Department of Chemical Engineering, Tsinghua University, Beijing 100084, China

ARTICLE INFO

Article history:
Received 18 May 2022
Received in revised form 6 August 2022
Accepted 7 August 2022
Available online 20 October 2022

Keywords:
Fuel cell
Hydrogen
Kinetics
Catalyst
CO_2 tolerance

ABSTRACT

Solid oxide fuel cells (SOFCs) that operate at intermediate temperatures of 600 to 800 °C have recently received increased attention due to their improved durability, more rapid startup and shutdown, better sealing and lower cost than their counterparts operate at high temperatures. Nevertheless, intermediate-temperature SOFCs (IT-SOFCs) with popular perovskite cathodes contain alkaline-earth elements, which are prone to reaction with carbon dioxide (CO_2), even when the CO_2 content is comparatively low. In this work, an alkaline-earth metal-free Ruddlesden–Popper oxide, $Nd_{1.8}La_{0.2}Ni_{0.74}Cu_{0.21}Ga_{0.05}O_{4+\delta}$ (NLNCG), is developed for IT-SOFC cathodes. The cell is based on an electrolyte with 8% (mol) Y_2O_3-stabilized ZrO_2 (8YSZ). The NLNCG cathode exhibits an excellent CO_2 tolerance, as proven by thermogravimetry analysis, *in situ* X-ray diffraction, I-V-P test, and electrochemical impedance spectroscopy (EIS), and stability measurements. The anode-supported single-cell NiO-YSZ|YSZ|NLNCG outputs a peak power density of 0.522 W·cm^{-2} at 800 °C. These findings suggest that NLNCG could be a highly suitable cathode material with CO_2 tolerance for IT-SOFCs.

1. Introduction

Solid oxide fuel cells (SOFCs) have been the focus of tremendous attention because they are environmentally friendly and efficient devices for directly converting the chemical energy that is stored in chemical fuels (such as hydrogen, hydrocarbons, ammonia, ethanol and carbon) into electrical energy [1–10]. However, the high operating temperatures (above 800 °C) of traditional SOFCs lead to many problems, such as interfacial chemical reactions, electrode sintering, poor durability and high-cost components [11,12]. Therefore, efforts are being made to decrease the operating temperature of SOFCs. However, the oxygen reduction reaction (ORR) kinetics of cathode materials weaken significantly at lower operating temperatures [12]. Lanthanum strontium cobalt ferrite (LSCF) and barium strontium cobalt ferrite (BSCF), which are mixed ionic and electron conductors (MIECs) with perovskite structures, exhibit high ORR kinetics and have been intensively investigated [13–18]. Unfortunately, alkaline-earth elements containing perovskite oxides have been reported to readily react with CO_2 at relatively low concentrations [19–24]. This poor CO_2 tolerance has been attributed to the strong basicity of the alkaline earth metals, as explained by Lewis acid-base theory, which react with acidic CO_2 gas [25–27]. For the commercialization of SOFCs, exploiting new, CO_2-tolerant cathodes is urgent and necessary.

In the past several decades, alkaline earth metal-free MIECs, which are members of the Ruddlesden–Popper series, with the K_2NiF_4-type structure and the chemical formula $A_{n+1}B_nO_{3n+1}$ (n = 1, 2, 3,⋯), have received much attention for oxygen separation and as IT-SOFC cathodes [28–41]. When n = 1, the oxygen-excess K_2NiF_4-type oxide $A_2BO_{4+\delta}$, which exhibits interactivity among its layers of perovskite ABO_3 and rock salt in the c-direction, can provide high mixed oxygen ionic and electronic conductivity [42]. In a previous study, we used a K_2NiF_4-type oxide named $Pr_{1.8}La_{0.2}Ni_{0.74}Cu_{0.21}Ga_{0.05}O_{4+\delta}$ (PLNCG) as a CO_2-tolerant negative electrode for a SOFC [43]. However, its ORR kinetics are limited and need further improvement. The Nd—O possesses lower bond energy than that of Pr—O, which enhances the ORR kinetics [44]. For instance, Sadykov *et al.* [45] observed lower polarization resistance for the Nd substituted $Nd_2NiO_{4+\delta}$ than that of $Pr_2NiO_{4+\delta}$ in SOFC. Therefore, in this work, Nd was chosen to completely substitute Pr to develop a new cathode material, namely, $Nd_{1.8}La_{0.2}Ni_{0.74}Cu_{0.21}Ga_{0.05}O_{4+\delta}$ (NLNCG), which exhibits satisfactory ORR kinetics and excellent

* Corresponding author.
E-mail address: xuejian@scut.edu.cn (J. Xue).

https://doi.org/10.1016/j.cjche.2022.08.023
1004-9541/

structural and performance stabilities in an atmosphere that includes CO_2.

2. Experimental

2.1. Powder preparation

The sol–gel method was used to produce powders as described in our previous research [46,47]. For NLNCG, stoichiometric amounts of raw analytical grade nitrates of Nd, La, Ni, Cu and Ga were dissolved in deionized water. After that, citric acid (CA) and $C_{10}H_{16}N_2O_8$ (EDTA) were added to the solution. The total metal ion:EDTA:CA molar ratio was 1:1:1.5. Aqueous ammonia was applied to regulate the pH to approximately 7. The mixture was then heated at 150 °C to obtain a gel, burned to acquire the NLNCG precursor, and calcined at 950 °C for 10 h to obtain the NLNCG powder.

2.2. Cell fabrication

The 8% (mol) Y_2O_3-stabilized ZrO_2 (8YSZ) was chosen as the electrolyte layer due to its good stability in H_2 between the temperature of 600 to 800 °C to avoid possible short circuits above 600 °C [48,49]. To fabricate the symmetrical cell NLNCG|YSZ|NLNCG, first, 0.5 g of YSZ powder that was purchased from the Ningbo Institute of Material Technology and Engineering was uniaxially pressed into a circular pellet at 10 MPa and fired at 1450 °C for 10 h to obtain a gas-tight YSZ electrolyte. Then, the NLNCG powder was mixed with a terpinol solution (containing 6% (mass) ethylcellulose) to form the cathode painting slurry. The NLNCG slurry was brush-painted on both sides of the YSZ and co-sintered at 850 °C for 3 h to fabricate the symmetrical cell. The PLNCG|YSZ|PLNCG symmetrical cell was fabricated using a similar process.

For the single-cell fabrication, the NiO, YSZ and starch powders with a mass ratio of 6:4:1 were ball milled in an ethanol media at 350 r·min^{-1} for 12 h to achieve uniform mixing. The starch powder was used as a pore former for the anode. Then, 0.5 g of the NiO-YSZ-starch powder mixture was uniaxially pressed into a circular pellet at 6 MPa, followed by heating to 1250 °C and retaining for 2 h to finish the anode support. YSZ was dip-coated on both sides of the anode [50,51]. The electrolyte was applied to both sides of the anode support to minimize asymmetrical thermal stress issues during sintering. The YSZ slurry consisted of YSZ, a 6% (mass) terpinol solution and ethanol with a mass ratio of 1:0.25:10 and was used for dip-coating. After drying the dip-coated YSZ electrolyte membrane at room temperature, the obtained YSZ|NiO-YSZ|YSZ pellet was treated at 1450 °C for 6 h. After co-sintering, the extra (thermal stress-compensating) YSZ electrolyte layer was removed by grinding with sandpaper to prepare a NiO-YSZ|YSZ semicell. The NLNCG cathode was compacted on the electrolyte by brush painting. Finally, the triple layers were cofired at 850 °C for 3 h to finish the NiO-YSZ|YSZ|NLNCG cell. The effect area of the cathodes was about 0.2 cm^2. Silver paste (DAD-87) was used to collect the current. Silver wire was adhered with silver paste to facilitate the connection of the cell to the electrochemical workstation.

2.3. Characterization

X-ray diffraction (XRD) patterns were investigated with a Bruker D8 ADVANCE diffractometer using Cu K_α radiation with the 2θ scanning angle changing from 20° to 80° at an interval of 0.02°. Thermogravimetry analysis (TGA) was performed with a NETZSCH STA 449F5 analyzer between room temperature (RT) and 1200 °C with a 10 °C·min^{-1} heating and cooling rate. A scanning electron microscope (SEM, HITACHI SU8200) was used to observe the anode-supported cell microstructure.

2.4. Electrochemical measurements

Electrochemical measurements were performed using an AUTOLAB instrument (Gamry Interface 1010). The electrical conductivity of NLNCG was tested with a constant voltage of 0.1 V. Electrochemical impedance spectroscopy (EIS) was performed under open circuit voltage (OCV) conditions. The applied frequency range was 0.1 Hz to 1 MHz, and 50 mV was set as the amplitude. The relationship between the current density, voltage and power density of the anode-supported cell was determined using the linear sweep mode from OCV to 0.2 V. The SOFC performance was studied in the temperature range from 600 to 800 °C, by feeding dry H_2 with a flow rate of 50 ml·min^{-1} in the anode and synthetic air with different CO_2 concentrations with a flow rate of 100 ml·min^{-1} in the cathode. The gas flow rates were calibrated by the mass-flow controllers (YIDUFLOW, MCF100-100SCCM).

3. Results and Discussion

The operating principle for oxygen ion-conducting SOFCs with fuel H_2 and oxidant O_2 is illustrated in Fig. 1. The O_2 at the cathode is first catalyzed to O^{2-} at the three-phase boundaries (O_2, O^{2-} and electron), and then the O^{2-} transfers through the O^{2-}-conducting electrolyte and reacts with H_2 at the anode. The electron that is

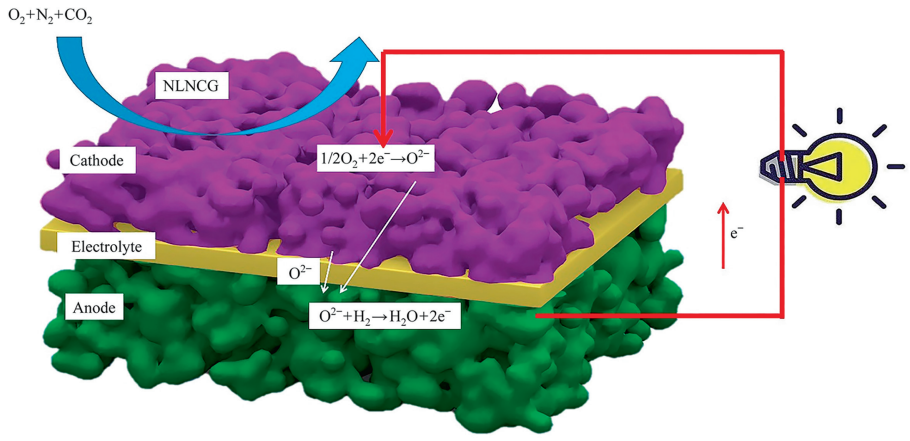

Fig. 1. Sketch map of the operating principle for oxygen ion-conducting SOFCs.

released from the oxidation of H_2 passes through the external circuit and arrives at the cathode. The process is described by the following equations:

$$\text{Cathode half-reaction}: \frac{1}{2}O_2 + 2e^- \rightarrow O^{2-} \quad (1)$$

$$\text{Anode half-reaction}: H_2 + O^{2-} \rightarrow H_2O + 2e^- \quad (2)$$

$$\text{Total reaction}: H_2 + \frac{1}{2}O_2 \rightarrow H_2O \quad (3)$$

3.1. Structure and micromorphology

NLNCG retained the K_2NiF_4-type structure after being fired at 950 °C for 10 h, despite the complete substitution of Pr by Nd in PLNCG, as shown in Fig. 2(a). A mixture of NLNCG and YSZ powders with a weight ratio of 1:1 was fired at 850 °C for 10 h to investigate the chemical compatibility of the two materials. All peaks were indexed to NLNCG and YSZ phases. No heterogeneous peaks appear, which indicates that no reaction occurrs between the NLNCG and YSZ powders during firing at 850 °C and they have excellent chemical compatibility, as shown in Fig. 2(b).

Furthermore, *in situ* XRD analysis was performed to investigate the phase stability of the NLNCG powder and the mixed NLNCG and YSZ powders under a CO_2 atmosphere at various temperatures. The heating and cooling rates were 10 °C·min^{-1}, and the holding time was 30 min before each measurement. As shown in Fig. 2(c) and (d), no additional reflections were observed during either the heating or cooling process, indicating their excellent CO_2 tolerance.

Then, the thermal stability of the NLNCG sample under both air and CO_2 atmospheres was investigated by TGA, as shown in Fig. S1 (a) (in Supplementary Material). The mass of the NLNCG sample under both air and CO_2 decreased slightly when the temperature increased due to the release of oxygen. The mass decrease under the air atmosphere was slower than that under CO_2 due to the

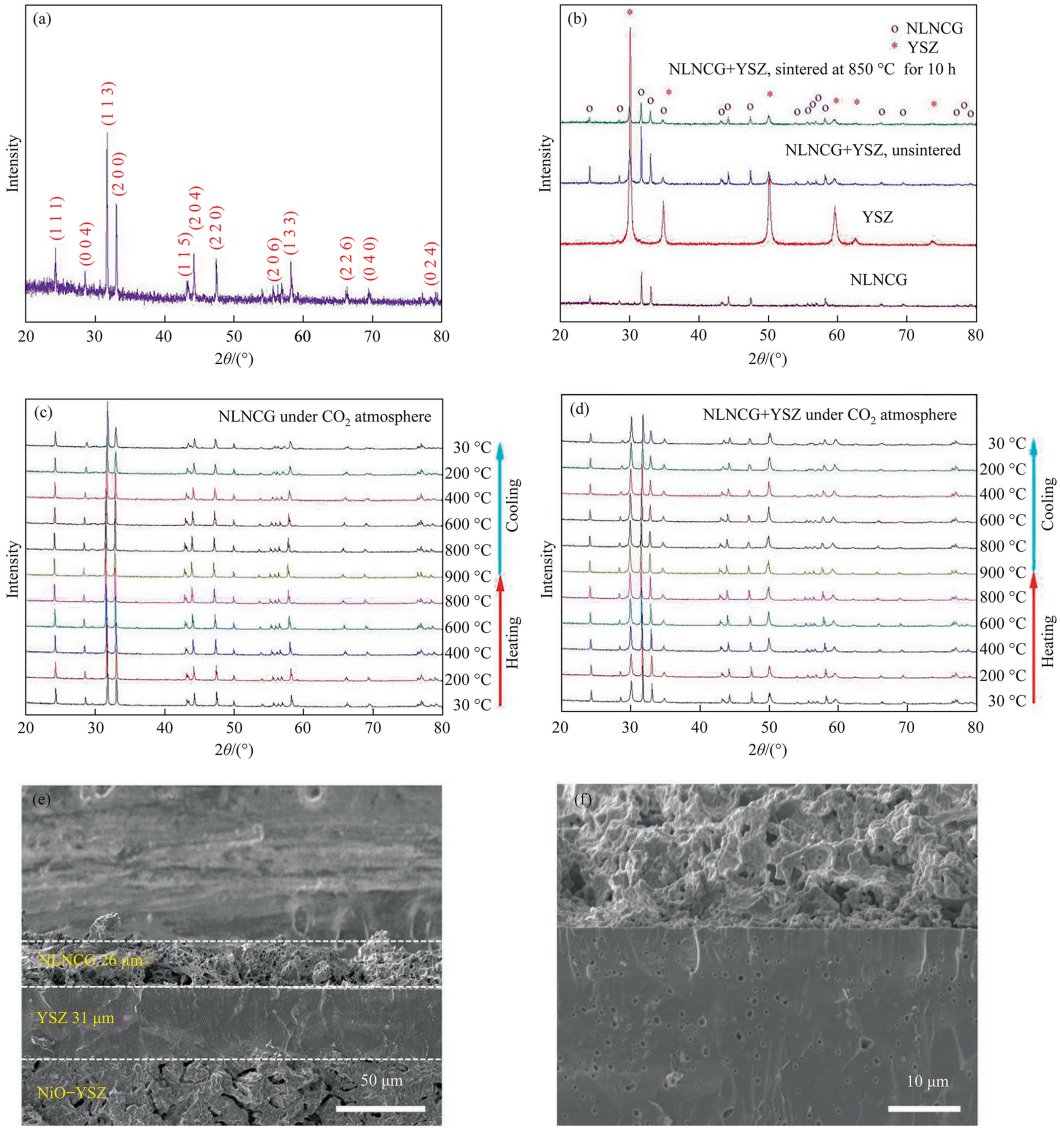

Fig. 2. Structures and micrographs of the powders and cells. Room-temperature XRD patterns of (a) the NLNCG precursor after sintering at 950 °C for 10 h and (b) the unsintered NLNCG-YSZ powder (mass ratio of 1:1) and this powder after sintering at 850 °C for 10 h; *in situ* XRD patterns of (c) NLNCG and (d) the NLNCG-YSZ mixture after heating from 30 to 900 °C and then cooling from 900 to 30 °C; (e) a cross-sectional view of a single-cell; and (f) an enlarged cross-sectional view of the YSZ electrolyte and NLNCG cathode.

higher oxygen partial pressure of air compared to CO_2. No mass increase from the formation of carbonates was observed, suggesting the excellent stability of NLNCG under the CO_2 atmosphere.

An anode-supported SOFC was constructed, and the microstructure of the cell is shown in Fig. S1(b) and Fig. 2(e) and (f). The YSZ electrolyte was dense and connected tightly with both electrodes, which favored a reduction in the contact resistance. Both the anode and cathode were porous, which was beneficial for gas diffusion to alleviate the concentration polarization of the electrode. The YSZ electrolyte layer was approximately 37 μm thick, which should decrease the O^{2-} transportation resistance of the electrolyte [52,53]. The NLNCG cathode layer, which had a thickness of approximately 24 μm, was beneficial for O_2 diffusion [54,55].

3.2. Electrochemical performance

The electrochemical performance of the samples and cells was also investigated, as shown in Fig. 3. Electrical conductivity is crucial for the cathode of a SOFC. Therefore, the electrical conductivity of NLNCG was examined in detail. Fig. 3(a) shows the total electrical conductivities of NLNCG under air, He, and CO_2 atmospheres. The electrical conductivity of NLNCG was positively correlated with temperature between 100 °C and 200 °C, indicating semiconductor-like behavior. The electrical conductivity attained a peak value of 35 $S \cdot cm^{-1}$ in the air at approximately 200 °C, and this value decreased at higher temperatures, thereby indicating metallic conductor behavior [56,57]. When the oxygen partial pressure decreased, the electrical conductivity decreased. The electrical conductivities of NLNCG under He and CO_2 atmospheres were relatively similar, thereby suggesting that CO_2 is harmless to the electrical conductivity of NLNCG. The electrical conductivity results of NLNCG under different atmospheres demonstrate that it is suitable for application as an SOFC cathode with CO_2 tolerance.

Table 1
PPDs of the SOFCs in this work and other literatures

Cathode	Temperature/ °C	PPD/ $W \cdot cm^{-2}$	Reference
$BaCo_{0.4}Fe_{0.4}Zr_{0.1}Y_{0.1}O_{3-\delta}$	800	0.512	[61]
$La_{0.6}Sr_{0.4}Co_{0.2}Fe_{0.8}O_{3-\delta}$	800	0.45	[62]
$(La_{0.6}Sr_{0.4})_{0.95}Co_{0.2}Fe_{0.8}O_{3-\delta}$	800	0.22	[63]
$Y_{0.06}Zr_{0.94}O_2$-$(La_{0.8}Sr_{0.2})_{0.95}MnO_3$	800	0.064	[64]
$Ba_{0.5}Sr_{0.5}Co_{0.8}Fe_{0.2}O_{3-\delta}$-$Ce_{0.8}Gd_{0.2}O_{1.9}$	800	0.34	[65]
$(La_{0.8}Sr_{0.2})_{0.95}MnO_{3-x}$-$Y_{0.16}Zr_{0.84}O_2$	800	0.3	[66]
$La_{0.6}Sr_{0.4}Co_{0.2}Fe_{0.8}O_{3-\delta}$	750	0.0241	[67]
$Ba_{0.5}Sr_{0.5}Co_{0.8}Fe_{0.2}O_{3-\delta}$-$Ce_{0.8}Gd_{0.2}O_{1.9}$	800	0.37	[68]
$La_{0.6}Ca_{0.3}Ce_{0.1}Mn_{1-x-y}Ni_xCr_yO_{3-\delta}$ $(x + y < 0.01)$	800	0.1	[69]
$La_{0.8}Sr_{0.2}MnO_{3-\delta}$-$Y_{0.16}Zr_{0.84}O_2$	800	0.149	[70]
$Nd_{1.8}La_{0.2}Ni_{0.74}Cu_{0.21}Ga_{0.05}O_{4+\delta}$	800	0.522	This work

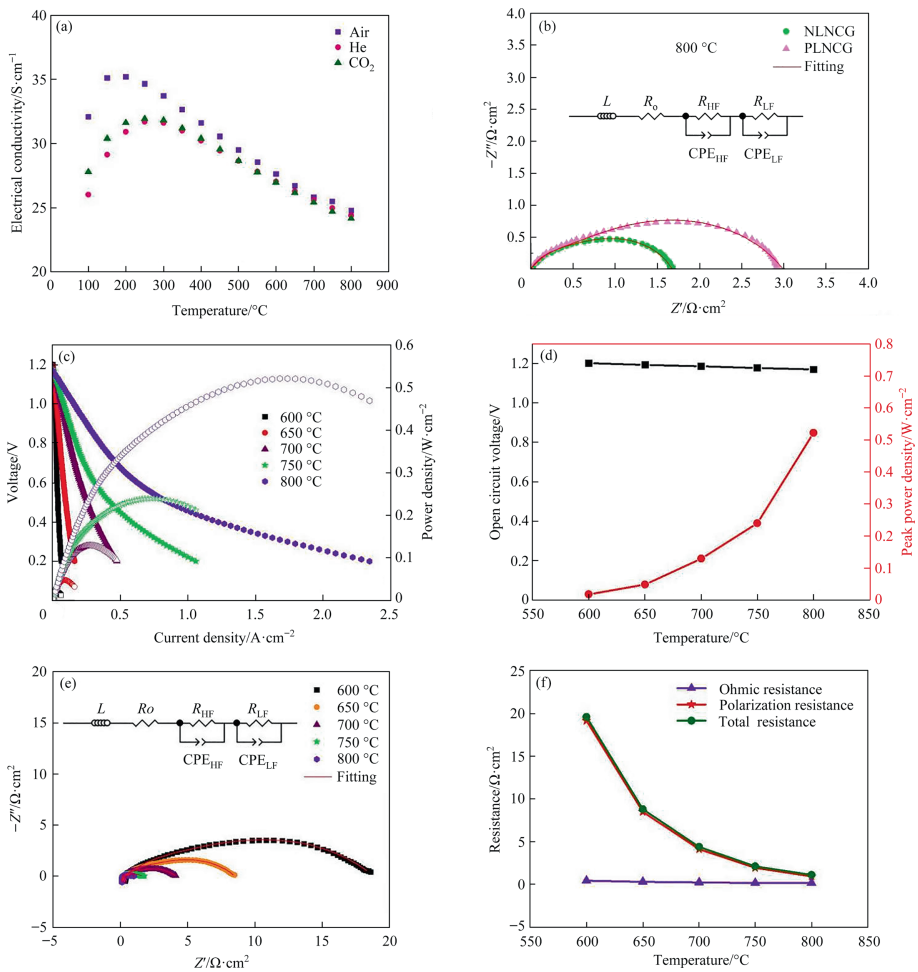

Fig. 3. The (a) electrical conductivity of the NLNCG sample between 100 and 800 °C in air, He and CO_2, (b) Nyquist plots of EIS of the NLNCG|YSZ|NLNCG and PLNCG|YSZ|PLNCG symmetrical cells in the air at 800 °C, (c) I–V characteristics and related power densities of the anode-supported SOFC NiO-YSZ|YSZ|NLNCG at various temperatures, (d) the derived OCVs and PPDs, (e) EIS of the anode-supported pellet SOFC NiO-YSZ|YSZ|NLNCG under OCV, and (f) the derived ohmic, polarization and total resistances. The insets in both Fig. 3(b) and (e) are the equivalent circuits for fitting the EIS.

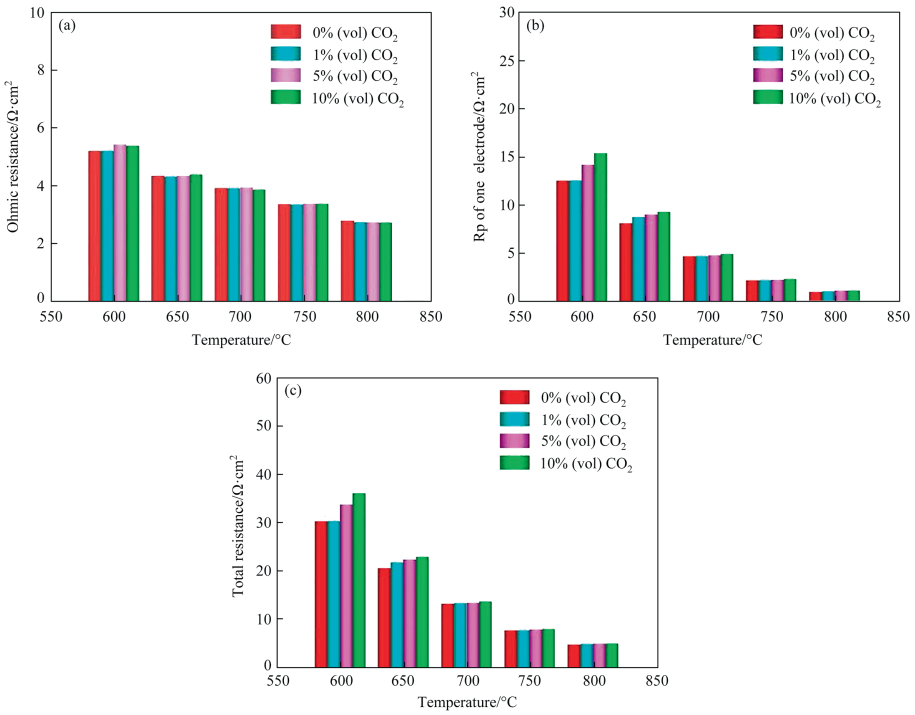

Fig. 4. Impacts of the CO_2 content on the (a) ohmic, (b) polarization and (c) total resistances of the symmetrical cell between 600 and 800 °C.

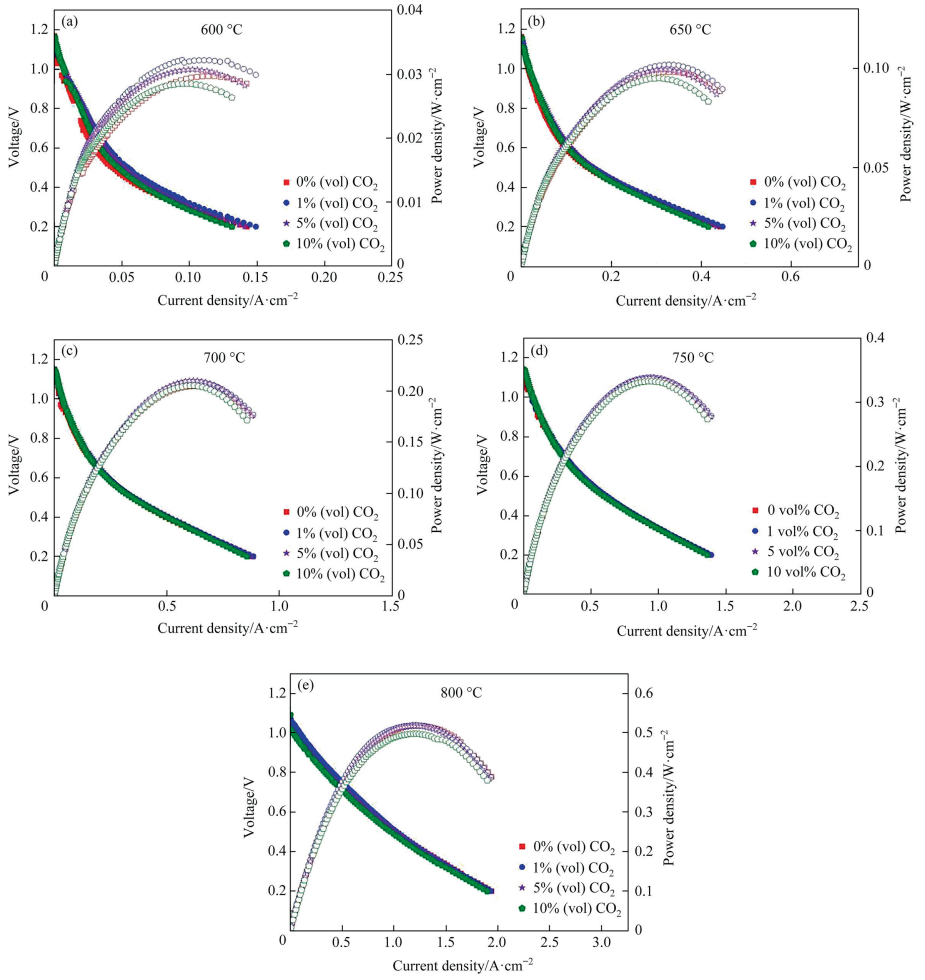

Fig. 5. I-V characteristics and related power densities of the anode-supported SOFC NiO-YSZ|YSZ|NLNCG at various temperatures and CO_2 concentrations.

To evaluate the initial ORR activities of the NLNCG and PLNCG cathodes, EIS tests were carried out using symmetrical cells under air at 700, 750 and 800 °C. The results are shown in Figs. 3(b) and S2. For PLNCG, the polarization resistance values were 1.47, 3.115 and 7.42 Ω·cm^2 at 800, 750 and 700 °C, respectively. For NLNCG, the values were 0.84, 1.35 and 2.7 Ω·cm^2, respectively. Therefore, the polarization resistance values of NLNCG were reduced by approximately 43%, 57% and 64% compared to those of PLNCG at 800, 750 and 700 °C, respectively, thereby demonstrating that Pr completely substituted by Nd has a favorable effect on the electrochemical performance. The EIS were fitted by the ZView software with an equivalent circuit L-Ro-(R_{HF}//CPE_{HF})-(R_{LF}//CPE_{LF}), as shown in the inset of Fig. 3(b). L, R and CPE represent inductance, resistance and constant phase element, respectively [58].

The I–V characteristics and the connected power densities of the anode-supported cell are illustrated in Fig. 3(c). The anode-supported SOFC output PPDs of 0.018, 0.048, 0.129, 0.24 and 0.522 W·cm^{-2} at 600, 650, 700, 750 and 800 °C, respectively. The extended reaction sites of the entire cathode surface of the MIEC compared to the triple-phase boundaries (TPBs) in pure electron conductors (such as $La_xSr_{1-x}MnO_{3-\delta}$) improved the cathode ORR kinetics, which enhanced the cell performance [59,60]. The PPDs of the SOFCs in this work and other literatures were listed in Table 1 for comparison, suggesting that the SOFCs with $Nd_{1.8}La_{0.2}Ni_{0.74}Cu_{0.21}Ga_{0.05}O_{4+\delta}$ cathode output the highest PPDs than that reported in references [61–70]. The OCVs of the cell were 1.201, 1.194, 1.186, 1.179 and 1.17 V at 600, 650, 700, 750 and 800 °C, respectively, which decreased as the temperature increased. All the OCV values were extremely close to the theoretical values that were calculated using the Nernst formula, thereby suggesting that the YSZ electrolyte was gas-tight. All the OCV and PPD values are summarized in Fig. 3d for direct comparison.

The EIS of the anode-supported cell is demonstrated in Fig. 3(e). The high frequency (HF) intercept reflects the electron conductivity of the electrodes, the oxygen ion conductivity, and the contact resistance of the interfaces, which is named the ohmic resistance of the cell [50]. Moreover, the low frequency (LF) intercept indicates the total cell resistance [51]. The electrode polarization resistance is the discrepancy between the two resistances. Therefore, at 600, 650, 700, 750 and 800 °C, the ohmic resistances were 0.458, 0.327, 0.256, 0.183 and 0.167 Ω·cm^2, and the polarization resistances were 19.139, 8.485, 4.137, 1.933 and 0.935 Ω·cm^2, respectively. All the resistance values are summarized in Fig. 3(f) for direct comparison.

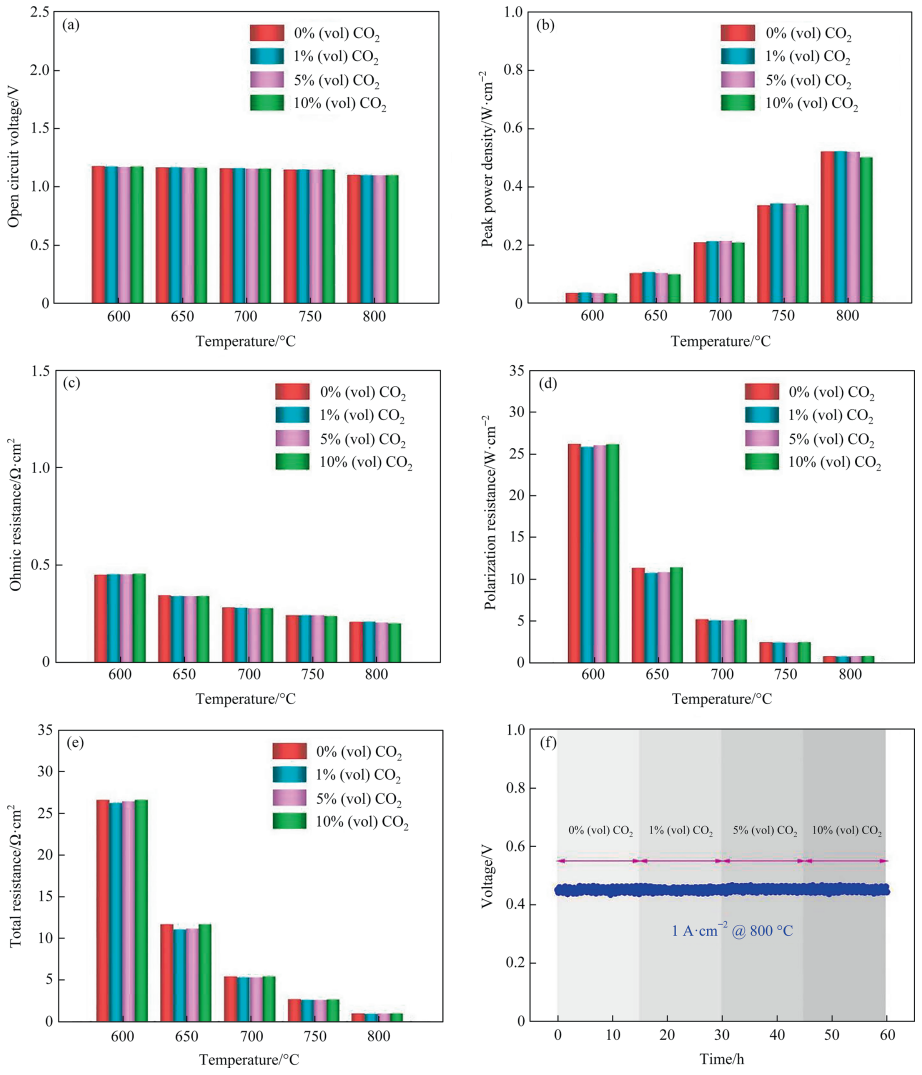

Fig. 6. Impacts of the CO_2 content on the (a) OCVs, (b) PPDs, (c) ohmic, (d) polarization and (e) total resistances of the single-cell between 600 and 800 °C, (f) the voltages of a single-cell that operating at a constant current density of 1 A·cm^{-2} at 800 °C.

3.3. CO_2 tolerance

To demonstrate the CO_2 tolerance of the NLNCG cathode, EIS measurements of a symmetrical cell and stability tests of a single-cell at different CO_2 concentrations were performed, and the results are shown in Fig. 4. Fig. S3 shows the initial EIS data of the symmetrical cell at various CO_2 concentrations between 600 and 800 °C, and the key data are shown in Fig. 4(a)–(c). As shown in Fig. 4(a), CO_2 has almost no impact on the ohmic resistance of the cell, thereby suggesting that there is no insulated carbonate formation on the NLNCG cathode. From Fig. 4(b), the polarization resistance values of the cell increased slightly as the CO_2 concentration increased at 600 and 650 °C, which was possibly due to the competitive adsorption between CO_2 and O_2 on the surface of the cathode. This kind of competitive adsorption weakened as the temperature increased. Between 700 and 800 °C, the influence of the CO_2 concentration on the total resistance values of the NLNCG cathode is small, as shown in Fig. 4(c).

To further evaluate the CO_2 tolerance of the NLNCG cathode, the I-V-P characteristics and EIS of the anode-supported cell at various temperatures and CO_2 concentrations were measured, as shown in Figs. 5 and S4. All the I-V, I-P and EIS curves exhibited high repeatability at the same temperature despite the CO_2 concentration changing from 0 to 10% (vol). The critical data of Figs. 5 and S4, such as OCV, PPD, ohmic, polarization and total resistances, were derived in Fig. 6(a)–(e) for direct comparison. Finally, the anode-supported cell with the NLNCG cathode was exposed to air with various CO_2 contents, and its stability was studied. Fig. 6(f) presents the impact of the CO_2 content on the voltage when the cell was operated at a constant current density of 1 $A{\cdot}cm^{-2}$ and temperature of 800 °C. As shown in Fig. 6(f), the cell performed stably with the voltage of about 0.45 V, when the CO_2 content gradually increased from 0 to 1%, 5% and 10% (vol). The abovementioned results indicate that the NLNCG could be a promising cathode material for IT-SOFCs under CO_2-containing conditions.

4. Conclusions

A K_2NiF_4-type oxide, namely NLNCG, was studied as a CO_2-tolerant cathode for IT-SOFCs. NLNCG was chemically compatible with YSZ and exhibited a preferable electrical conductivity between 600 and 800 °C in air. The polarization resistance values of the NLNCG cathode were reduced by approximately 43%, 57% and 64% compared to those of the PLNCG cathode at 800, 750 and 700 °C, respectively. The PPD was 0.522 $W{\cdot}cm^{-2}$ for the NiO-YSZ|YSZ|NLNCG SOFC. Both the EIS measurement results of the NLNCG|YSZ|NLNCG electrolyte-supported symmetrical cell and the stability test results of the NiO-YSZ|YSZ|NLNCG anode-supported cell reveal the excellent CO_2 tolerance of the NLNCG cathode between 600 and 800 °C. The results suggest that NLNCG could be a highly suitable cathode material with CO_2 tolerance for IT-SOFCs.

Declaration of Competing Interest

The authors declare that they have no known competing financial interests or personal relationships that could have appeared to influence the work reported in this paper.

Acknowledgements

The authors greatly acknowledge the financial support by the National Key Research and Development Program of China (2020YFB1505603), the National Natural Science Foundation of China (22075086), the Guangdong Basic and Applied Basic Research Foundation (2020A1515011157, 2022A1515010980) and the Doctor Scientific Research Startup Foundation of Jinggangshan University (JZB1324).

Supplementary Material

Supplementary data to this article can be found online at https://doi.org/10.1016/j.cjche.2022.08.023.

References

[1] C.Y. Ai, T.T. Li, R.Z. Ren, Z.H. Wang, W. Sun, J.S. Feng, K.N. Sun, J.S. Qiao, Barium-doped $Pr_2Ni_{0.6}Cu_{0.4}O_{4+\delta}$ with triple conducting characteristics as cathode for intermediate temperature proton conducting solid oxide fuel cell, *Chin. J. Chem. Eng.* 39 (2021) 269–276.
[2] C.C. Duan, J.H. Tong, M. Shang, S. Nikodemski, M. Sanders, S. Ricote, A. Almansoori, R. O'Hayre, Readily processed protonic ceramic fuel cells with high performance at low temperatures, *Science* 349 (6254) (2015) 1321–1326.
[3] Y. Zhang, B. Chen, D. Guan, M. Xu, R. Ran, M. Ni, W. Zhou, R. O'Hayre, Z. Shao, Thermal-expansion offset for high-performance fuel cell cathodes, *Nature* 591 (2021) 246–251.
[4] G. Kobayashi, Y. Hinuma, S. Matsuoka, A. Watanabe, M. Iqbal, M. Hirayama, M. Yonemura, T. Kamiyama, I. Tanaka, R. Kanno, Pure H^- conduction in oxyhydrides, *Science* 351 (6279) (2016) 1314–1317.
[5] L. Yang, S.Z. Wang, K. Blinn, M.F. Liu, Z. Liu, Z. Cheng, M.L. Liu, Enhanced sulfur and coking tolerance of a mixed ion conductor for SOFCs: $BaZr_{0.1}Ce_{0.7}Y_{0.2-x}Yb_xO_{3-\delta}$, *Science* 326 (5949) (2009) 126–129.
[6] J.-H. Myung, D. Neagu, D.N. Miller, J.T. Irvine, Switching on electrocatalytic activity in solid oxide cells, *Nature* 537 (2016) 528–531.
[7] M. Ni, Z.P. Shao, Fuel cells that operate at 300° to 500 °C, *Science* 369 (6500) (2020) 138–139.
[8] J.X. Peng, J. Huang, X.-L. Wu, Y.-W. Xu, H.C. Chen, X. Li, Solid oxide fuel cell (SOFC) performance evaluation, fault diagnosis and health control: A review, *J. Power Sources* 505 (2021) 230058.
[9] H.G. Shi, Q.J. Li, W.Y. Tan, H. Qiu, C. Su, Solid oxide fuel cells in combination with biomass gasification for electric power generation, *Chin. J. Chem. Eng.* 28 (4) (2020) 1156–1161.
[10] L.J. Tan, C. Yang, N.N. Zhou, Synthesis/design optimization of SOFC-PEM hybrid system under uncertainty, *Chin. J. Chem. Eng.* 23 (1) (2015) 128–137.
[11] X.L. Liu, F.J. Jin, X.W. Liu, N. Sun, J.X. Li, Y. Shen, F. Wang, L. Yang, X.Y. Chu, M.Z. Xu, Y.J. Zhai, J.H. Li, Effect of calcium doping on $Sm_{1-x}Ca_xBaCo_2O_{5+\delta}$ cathode materials for intermediate-temperature solid oxide fuel cells, *Electrochim. Acta* 390 (2021) 138830.
[12] Z.H. Du, K.Y. Li, H.L. Zhao, X. Dong, Y. Zhang, K. Świerczek, A $SmBaCo_2O_{5+\delta}$ double perovskite with epitaxially grown $Sm_{0.2}Ce_{0.8}O_{2-\delta}$ nanoparticles as a promising cathode for solid oxide fuel cells, *J. Mater. Chem. A* 8 (2020) 14162–14170.
[13] W. Zhou, R. Ran, Z.P. Shao, Progress in understanding and development of $Ba_{0.5}Sr_{0.5}Co_{0.8}Fe_{0.2}O_{3-\delta}$-based cathodes for intermediate-temperature solid-oxide fuel cells: A review, *J. Power Sources* 192 (2) (2009) 231–246.
[14] H.Q. Xie, Y.Y. Wei, H.H. Wang, Modeling of U-shaped $Ba_{0.5}Sr_{0.5}Co_{0.8}Fe_{0.2}O_{3-\delta}$ hollow-fiber membrane for oxygen permeation, *Chin. J. Chem. Eng.* 25 (7) (2017) 892–897.
[15] A.M. Asensio, D. Clematis, M. Viviani, M.P. Carpanese, S. Presto, D. Cademartori, P.L. Cabot, A. Barbucci, Impregnation of microporous SDC scaffold as stable solid oxide cell BSCF-based air electrode, *Energy* 237 (2021) 121514.
[16] M. Shah, S.A. Barnett, Solid oxide fuel cell cathodes by infiltration of $La_{0.6}Sr_{0.4}Co_{0.2}Fe_{0.8}O_{3-\delta}$ into Gd-Doped Ceria, *Solid State Ion.* 179 (35–36) (2008) 2059–2064.
[17] A. Esquirol, N.P. Brandon, J.A. Kilner, M. Mogensen, Electrochemical characterization of $La_{0.6}Sr_{0.4}Co_{0.2}Fe_{0.8}O_3$ cathodes for intermediate-temperature SOFCs, *J. Electrochem. Soc.* 151 (11) (2004) A1847–A1855.
[18] J. Song, C. Li, S. Zhang, X.X. Meng, B. Meng, J. Sunarso, Catalyst-modified perovskite hollow fiber membrane for oxidative coupling of methane, *Chin. J. Chem. Eng.* 41 (2022) 412–419.
[19] A.Y. Yan, M.J. Cheng, Y.L. Dong, W.S. Yang, V. Maragou, S.Q. Song, P. Tsiakaras, Investigation of a $Ba_{0.5}Sr_{0.5}Co_{0.8}Fe_{0.2}O_{3-\delta}$ based cathode IT-SOFC I. The effect of CO_2 on the cell performance, *Appl. Catal. B-Environ.* 66 (1–2) (2006) 64–71.
[20] A.Y. Yan, V. Maragou, A. Arico, M.J. Cheng, P. Tsiakaras, Investigation of a $Ba_{0.5}Sr_{0.5}Co_{0.8}Fe_{0.2}O_{3-\delta}$ based cathode SOFC II. The effect of CO_2 on the chemical stability, *Appl. Catal. B-Environ.* 76 (3–4) (2007) 320–327.
[21] A.Y. Yan, M. Yang, Z.F. Hou, Y.L. Dong, M.J. Cheng, Investigation of $Ba_{1-x}Sr_xCo_{0.8}Fe_{0.2}O_{3-\delta}$ as cathodes for low-temperature solid oxide fuel cells both in the absence and presence of CO_2, *J. Power Sources* 185 (1) (2008) 76–84.
[22] J.X. Yi, M. Schroeder, T. Weirich, J. Mayer, Behavior of $Ba(Co, Fe, Nb)O_{3-\delta}$ perovskite in CO_2-containing atmospheres: Degradation mechanism and materials design, *Chem. Mater.* 22 (23) (2010) 6246–6253.
[23] Y.Q. Meng, L. Sun, J. Gao, W.Z. Tan, C.S. Chen, J.X. Yi, H.J.M. Bouwmeester, Z.H. Sun, K.S. Brinkman, Insights into the CO_2 Stability-performance trade-off of antimony-doped $SrFeO_{3-\delta}$ perovskite cathode for solid oxide fuel cells, *ACS Appl. Mater. Interfaces* 11 (12) (2019) 11498–11506.

[24] J.L. Wang, Z.B. Yang, L.M. Ba, Y. Chen, B. Ge, S.P. Peng, Effects of CO_2 and H_2O on $Ba_{0.9}Co_{0.7}Fe_{0.2}Nb_{0.1}O_{3-\delta}$ cathode and modification by a $Ce_{0.9}Gd_{0.1}O_{2-\delta}$ coating, *J. Electroanal. Chem.* 827 (2018) 79–84.

[25] B.B. Gu, J. Sunarso, Y. Zhang, Y.F. Song, G.M. Yang, W. Zhou, Z.P. Shao, A high performance composite cathode with enhanced CO_2 resistance for low and intermediate-temperature solid oxide fuel cells, *J. Power Sources* 405 (2018) 124–131.

[26] Y.J. Gou, G.D. Li, R.Z. Ren, C.M. Xu, J.S. Qiao, W. Sun, K.N. Sun, Z.H. Wang, Pr-doping motivating the phase transformation of the $BaFeO_{3-\delta}$ perovskite as a high-performance solid oxide fuel cell cathode, *ACS Appl. Mater. Interfaces* 13 (17) (2021) 20174–20184.

[27] D.M. Huan, L. Zhang, K. Zhu, X.Y. Li, B.Z. Zhang, J.L. Shi, R.R. Peng, C.R. Xia, Tailoring the structural stability, electrochemical performance and CO_2 tolerance of aluminum doped $SrFeO_3$, *Sep. Purif. Technol.* 290 (2022) 120843.

[28] J. Xue, Q. Liao, W. Chen, H.J.M. Bouwmeester, H.H. Wang, A. Feldhoff, A new CO_2-resistant Ruddlesden-Popper oxide with superior oxygen transport: A-site deficient $(Pr_{0.9}La_{0.1})_{1.9}(Ni_{0.74}Cu_{0.21}Ga_{0.05})O_{4+\delta}$, *J. Mater. Chem. A* 3 (2015) 19107–19114.

[29] J. Xue, J.Q. Li, L.B. Zhuang, L. Chen, A. Feldhoff, H.H. Wang, Anion doping CO_2-stable oxygen permeable membranes for syngas Production, *Chem. Eng. J.* 347 (2018) 84–90.

[30] E. Pikalova, A. Kolchugin, K. Zakharchuk, D. Boiba, V. Tsvinkinberg, E. Filonova, A. Khrustov, A. Yaremchenko, Mixed ionic-electronic conductivity, phase stability and electrochemical activity of Gd-substituted $La_2NiO_{4+\delta}$ as oxygen electrode material for solid oxide fuel/electrolysis cells, *Int. J. Hydrog. Energy* 46 (32) (2021) 16932–16946.

[31] R. Dutta, A. Maity, A. Marsicano, M. Ceretti, D. Chernyshov, A. Bosak, A. Villesuzanne, G. Roth, G. Perversika, W. Paulus, Long-range oxygen ordering linked to topotactic oxygen release in $Pr_2NiO_{4+\delta}$ fuel cell cathode material, *J. Mater. Chem. A* 8 (2020) 13987–13995.

[32] J.Q. Li, S. Lei, B.X. Deng, J. Xue, Y.J. Wang, H.H. Wang, Reducing anisotropic effects on oxygen separation performance of K_2NiF_4-type membranes by adjusting grain size, *J. Membr. Sci.* 618 (2021) 118628.

[33] J. Xue, A. Feldhoff, Ambient air partial internal reduction of NiO in a mixed ionic-electronic conducting ceramic, *J. Eur. Ceram. Soc.* 36 (14) (2016) 3451–3456.

[34] C.G. Yao, J.X. Yang, H.X. Zhang, S.G. Chen, J. Meng, K.D. Cai, Evaluation of bismuth doped $La_{2-x}Bi_xNiO_{4+\delta}$ (x = 0, 0.02 and 0.04) as cathode materials for solid oxide fuel cells, *Ceram. Int.* 47 (17) (2021) 24589–24596.

[35] R. Sayers, J. Liu, B. Rustumji, S.J. Skinner, Novel K_2NiF_4-type materials for solid oxide fuel cells: compatibility with electrolytes in the intermediate temperature range, *Fuel Cells* 8 (5) (2008) 338–343.

[36] J. Xue, A. Schulz, H.H. Wang, A. Feldhoff, The phase stability of the Ruddlesden-Popper type oxide $(Pr_{0.9}La_{0.1})_{2.0}Ni_{0.74}Cu_{0.21}Ga_{0.05}O_{4+\delta}$ in an oxidizing environment, *J. Membr. Sci.* 497 (2016) 357–364.

[37] Y.Y. Wei, Q. Liao, Z. Li, H.H. Wang, Enhancement of oxygen permeation through U-shaped K_2NiF_4-type oxide hollow fiber membranes by surface modifications, *Sep. Purif. Technol.* 110 (2013) 74–80.

[38] D. Cetin, S. Poizeau, J. Pietras, S. Gopalan, Decomposition of La_2NiO_4 in $Sm_{0.2}Ce_{0.8}O_2$-La_2NiO_4 composites for solid oxide fuel cell applications, *Solid State Ion.* 300 (2017) 91–96.

[39] S.J. Zhao, N. Li, L.P. Sun, Q. Li, L.H. Huo, H. Zhao, A novel high-entropy cathode with the A_2BO_4-type structure for solid oxide fuel cells, *J. Alloy. Compd.* 895 (1) (2022) 162548.

[40] Y. Chen, Q. Liao, Y.Y. Wei, Z. Li, H.H. Wang, A CO_2-stable K_2NiF_4-type oxide $(Nd_{0.9}La_{0.1})_2(Ni_{0.74}Cu_{0.21}Al_{0.05})O_{4+\delta}$ for oxygen separation, *Ind. Eng. Chem. Res.* 52 (25) (2013) 8571–8578.

[41] J. Banner, A. Akter, R.F. Wang, J. Pietras, S. Sulekar, O.A. Marina, S. Gopalan, Rare earth nickelate electrodes containing heavily doped ceria for reversible solid oxide fuel cells, *J. Power Sources* 507 (2021) 230248.

[42] C.N. Munnings, S.J. Skinner, G. Amow, P.S. Whitfield, I.J. Davidson, Oxygen transport in the $La_2Ni_{1-x}Co_xO_{4+\delta}$ system, *Solid State Ion.* 176 (23–24) (2005) 1895–1901.

[43] S.J. Peng, Y.Y. Wei, J. Xue, Y. Chen, H.H. Wang, $Pr_{1.8}La_{0.2}Ni_{0.74}Cu_{0.21}Ga_{0.05}O_{4+\delta}$ as a potential cathode material with CO_2 resistance for intermediate temperature solid oxide fuel cell, *Int. J. Hydrog. Energy* 38 (25) (2013) 10552–10558.

[44] Q. Zheng, J. Xue, Q. Liao, Y.Y. Wei, Z. Li, H.H. Wang, CO_2-tolerant alkaline-earth metal-free single phase membrane for oxygen separation, *Chem. Eng. Sci.* 101 (2013) 240–247.

[45] V.A. Sadykov, E.Y. Pikalova, A.A. Kolchugin, A.V. Fetisov, E.M. Sadovskaya, E.A. Filonova, N.F. Eremeev, V.B. Goncharov, A.V. Krasnov, P.I. Skriabin, A.N. Shmakov, Z.S. Vinokurov, A.V. Ishchenko, S.M. Pikalov, Transport properties of Ca-doped Ln_2NiO_4 for intermediate temperature solid oxide fuel cells cathodes and catalytic membranes for hydrogen production, *Int. J. Hydrog. Energy* 45 (25) (2020) 13625–13642.

[46] Y. Chen, H. Liu, L.B. Zhuang, Y.Y. Wei, H.H. Wang, Hydrogen permeability through $Nd_{5.5}W_{0.35}Mo_{0.5}Nb_{0.15}O_{11.25-\delta}$ mixed protonic-electronic conducting membrane, *J. Membr. Sci.* 579 (2019) 33–39.

[47] J. Xue, G.W. Weng, L. Chen, Y.P. Suo, Y.Y. Wei, A. Feldhoff, H.H. Wang, Various influence of surface modification on permeability and phase stability through an oxygen permeable membrane, *J. Membr. Sci.* 573 (2019) 588–594.

[48] Z.L. Zhan, S.A. Barnett, An octane-fueled solid oxide fuel cell, *Science* 308 (5723) (2005) 844–847.

[49] N. Jaiswal, K. Tanwar, R. Suman, D. Kumar, S. Upadhyay, O. Parkash, A brief review on ceria based solid electrolytes for solid oxide fuel cells, *J. Alloy. Compd.* 781 (2019) 984–1005.

[50] D.X. Zhou, S.J. Peng, Y.Y. Wei, Z. Li, H.H. Wang, Novel asymmetric anode-supported hollow fiber solid oxide fuel cell, *J. Alloy. Compd.* 523 (2012) 134–138.

[51] S.J. Peng, D.X. Zhou, Y.Y. Wei, Z. Li, H.H. Wang, A novel U-shaped anode-supported hollow fiber solid oxide fuel cell with considerable thermal cycling performance and stability, *J. Membr. Sci.* 417–418 (2012) 80–86.

[52] J.W. Fergus, Electrolytes for solid oxide fuel cells, *J. Power Sources* 162 (1) (2006) 30–40.

[53] D. Beckel, A. Bieberle-Hütter, A. Harvey, A. Infortuna, U.P. Muecke, M. Prestat, J. L.M. Rupp, L.J. Gauckler, Thin films for micro solid oxide fuel cells, *J. Power Sources* 173 (1) (2007) 325–345.

[54] J.Y. Koo, T. Mun, J. Lee, M. Choi, S.J. Kim, W. Lee, Enhancement of oxygen reduction reaction kinetics using infiltrated yttria-stabilized zirconia interlayers at the electrolyte/electrode interfaces of solid oxide fuel cells, *J. Power Sources* 472 (2020) 228606.

[55] J.Y. Ma, Y.X. Pan, Y.K. Wang, Y. Chen, A Sr and Ni doped Ruddlesden−Popper perovskite oxide $La_{1.6}Sr_{0.4}Cu_{0.6}Ni_{0.4}O_{4+\delta}$ as a promising cathode for protonic ceramic fuel cells, *J. Power Sources* 509 (2021) 230369.

[56] F.F. Lu, T. Xia, Q. Li, L.P. Sun, L.H. Huo, H. Zhao, Ta-doped $PrBa_{0.94}Co_{2-x}Ta_xO_{5+\delta}$ as promising oxygen electrodes: A focused study on catalytic oxygen reduction reaction activity, stability and CO_2-durability, *J. Power Sources* 417 (2019) 42–52.

[57] M. Yashima, N. Sirikanda, T. Ishihara, Crystal structure, diffusion path, and oxygen permeability of a Pr_2NiO_4-based mixed conductor $(Pr_{0.9}La_{0.1})_2(Ni_{0.74}Cu_{0.21}Ga_{0.05})O_{4+\delta}$, *J. Am. Chem. Soc.* 132 (7) (2010) 2385–2392.

[58] A. Giuliano, C. Nicollet, S. Fourcade, F. Mauvy, M.P. Carpanese, J.-C. Grenier, Influence of the electrode/electrolyte interface structure on the performance of $Pr_{0.8}Sr_{0.2}Fe_{0.7}Ni_{0.3}O_{3-\delta}$ as solid oxide fuel cell cathode, *Electrochim. Acta* 236 (2017) 328–336.

[59] X. Chen, H.L. Zhang, Y.Y. Li, J.Z. Xing, Z. Zhang, X. Ding, B. Zhang, J. Zhou, S.R. Wang, Fabrication and performance of anode-supported proton conducting solid oxide fuel cells based on $BaZr_{0.1}Ce_{0.7}Y_{0.1}Yb_{0.1}O_{3-\delta}$ electrolyte by multi-layer aqueous-based co-tape casting, *J. Power Sources* 506 (2021) 229922.

[60] Z.X. Lin, K. Zhao, G. Cheng, S.Z. Hu, M. Chen, J. Li, D.C. Chen, Q. Xu, M.L. Chang, O. Volodymyr, Catalyst layer supported solid oxide fuel cells running on methane, *J. Power Sources* 507 (2021) 230317.

[61] X.D. Xiong, J. Yu, X.J. Huang, D. Zou, Y.F. Song, M.G. Xu, R. Ran, W. Wang, W. Zhou, Z.P. Shao, Slightly ruthenium doping enables better alloy nanoparticle exsolution of perovskite anode for high-performance direct-ammonia solid oxide fuel cells, *J. Mater. Sci. Technol.* 125 (2022) 51–58.

[62] F.H. Zhang, Q.H. Weng, Y.X. Zhang, N. Ai, S.P. Jiang, C.Z. Guan, Y.Q. Shao, H.H. Fang, Y. Luo, K.F. Chen, Facile preparation of electrodes of efficient electrolyte-supported solid oxide fuel cells using a direct assembly approach, *Electrochim. Acta* 424 (2022) 140643.

[63] Y. Komatsu, A. Sciazko, N. Shikazono, Isostatic pressing of screen printed nickel-gadolinium doped ceria anodes on electrolyte-supported solid oxide fuel cells, *J. Power Sources* 485 (2021) 229317.

[64] H.L. Zhang, T. Chen, Z.Z. Huang, G.Z. Hu, J. Zhou, S.R. Wang, A cathode-supported solid oxide fuel cell prepared by the phase-inversion tape casting and impregnating method, *Int. J. Hydrog. Energy* 47 (43) (2022) 18810–18819.

[65] M.K. Rath, B.H. Choi, M.J. Ji, K.T. Lee, Eggshell-membrane-templated synthesis of hierarchically-ordered NiO-$Ce_{0.8}Gd_{0.2}O_{1.9}$ composite powders and their electrochemical performances as SOFC anodes, *Ceram. Int.* 40 (2) (2014) 3295–3304.

[66] T. Altan, C. Timurkutluk, B. Timurkutluk, Impact of lamination conditions on microtubular solid oxide fuel cells fabricated by tape casting coupled with isostatic pressing, *J. Power Sources* 532 (2022) 231369.

[67] Y.J. Shi, Y.T. Wen, K. Huang, X.L. Xiong, J. Wang, M.L. Liu, D. Ding, Y. Chen, T. Liu, Surface enhanced performance of $La_{0.6}Sr_{0.4}Co_{0.2}Fe_{0.8}O_{3-\delta}$ cathodes by infiltration Pr-Ni-Mn-O progress, *J. Alloy. Compd.* 902 (2022) 163337.

[68] C.K. Cho, B.H. Choi, K.T. Lee, Effect of Co alloying on the electrochemical performance of Ni-$Ce_{0.8}Gd_{0.2}O_{1.9}$ anodes for hydrocarbon-fueled solid oxide fuel cells, *J. Alloy. Compd.* 541 (2012) 433–439.

[69] X. Li, N. Xu, X. Zhao, K. Huang, Performance of a commercial cathode-supported solid oxide fuel cells prepared by single-step infiltration of an ion-conducting electrocatalyst, *J. Power Sources* 199 (2012) 132–137.

[70] K.J. Jia, L.N. Zheng, W. Liu, J.J. Zhang, F.Y. Yu, X.X. Meng, C. Li, J. Sunarso, N.T. Yang, A new and simple way to prepare monolithic solid oxide fuel cell stack by stereolithography 3D printing technology using 8 mol% yttria stabilized zirconia photocurable slurry, *J. Eur. Ceram. Soc.* 42 (10) (2022) 4275–4285.